JOURNAL OF MATERIALS SCIENCE **34** (1999) 4563–4572

Microstructure and properties of a composite system for dental applications composed of glass-ceramics in the SiO_2–Li_2O–ZrO_2–P_2O_5 system and ZrO_2-ceramic (TZP)

M. SCHWEIGER, M. FRANK, S. CRAMER VON CLAUSBRUCH, W. HÖLAND, V. RHEINBERGER
Ivoclar Ltd, Benderstrasse 2, FL 9494 Schaan, Principality of Liechtenstein
E-mail: marcel.schweiger@ivoclar.com

The objective of the study was to develop a biocompatible composite system which was composed of TZP-ceramic (tetragonal zirconia polycrystals, ZrO_2 stabilized with 3 mol % Y_2O_3) and two glass-ceramics of the SiO_2–Li_2O–ZrO_2–P_2O_5 type. The metal-free composite system would satisfy the translucency, the biocompatibility and the strength requirements of dentistry. The two glass-ceramics of the SiO_2–Li_2O–ZrO_2–P_2O_5 type with a content of 15 and 20 wt % ZrO_2 respectively, were chemically and physically adapted to TZP-ceramic. The glass-ceramics were used as a dentin buildup material. The TZP-ceramic had the function of a root post. The shape of the post was cylindrical with a conical tip. The composite system was easy to process through viscous flow of the glass-ceramic at 900 and 1000 °C, respectively. The microstructure and the mechanical properties of two glass-ceramics of the SiO_2–Li_2O–ZrO_2–P_2O_5 type were examined therefore.

1. Introduction

There is a strong trend towards metal-free restorations in modern dentistry. These restorations are providing an alternative for patients with metal allergies. Furthermore, they are also producing highly aesthetic results. Accordingly, biocompatibility and aesthetics are also an important issue in endodontics. To date, root posts for the reinforcement of remaining tooth structure have been made of metal alloys. Now, efforts are underway to replace the metal root posts with ones made of biocompatible materials [1, 2]. Moreover, in the past, the dentin core had to be reconstructed in a very complicated procedure using a ceramic or glass-ceramic material. In addition, the dark, opaque metal post produce an undesirable greyish shade in restored teeth, particularly in the anterior region. The objective of this study, therefore, was to develop a biocompatible metal-free composite system with which the translucency and strength of natural teeth can be simulated.

The composite system was composed of TZP ceramic (tetragonal zirconia polycrystals, ZrO_2 stabilized with 3 mol % Y_2O_3) in the form of a cylindrical root post with a conical tip and a chemically and physically adapted glass-ceramic of the SiO_2-ZrO_2-Li_2O-P_2O_5-type for the dentin core buildup. Highly aesthetic, mechanically stable restorations were produced with these materials [3–7].

TZP ceramic has already been clinically proven in implantology. The ceramic demonstrates high flexural strength and fracture toughness [8]. These properties are achieved with transformation toughening [9]. The innovative feature of the dental application presented in this article is the use of a glass-ceramic that demonstrates adjusted thermal expansion and a high ZrO_2-content to produce an optimum bond with the ZrO_2 ceramic.

Glass-ceramics containing ZrO_2 crystals are already being used for technical, non-medical applications [10–14]. Although these glass-ceramics demonstrate favourable mechanical properties, they are highly opaque. The translucency and strength of the materials produced from the SiO_2–Li_2O–ZrO_2–P_2O_5 system can be controlled to suit specific dental applications.

2. Experimental

2.1. Material

The ZrO_2-posts were produced by cold isostatic pressing, sintering and additional hot isostatic pressing to achieve defect-free sintered parts [15].

Two glass-ceramics demonstrating different compositions derived from the SiO_2–Li_2O–ZrO_2–P_2O_5 system were studied. The glass-ceramics were labelled A and B. Table I shows the composition of the base glasses.

Sintered glass-ceramic ingots were used for the production of test specimens and dental restorations. The glass-ceramic ingots were pressed in a mould by viscous flow through heat and pressure.

TABLE I Composition of glass-ceramic A and B

Component (wt %)	Glass-ceramic A	Glass-ceramic B
SiO_2	58.7	50.8
Li_2O	8.0	8.3
ZrO_2	15.2	20.1
P_2O_5	4.2	10.0
Al_2O_3	5.0	2.9
Na_2O	3.2	2.8
K_2O	4.8	4.3
F	1.0	0.9

2.2. Production of glass-ceramic ingots

A glass consisting of oxides, carbonates, phosphates, and fluorides was melted to form the base material for manufacturing the glass-ceramic. The raw materials were homogeneously blended and melted in a Pt/Rh crucible at 1500 °. Homogenization took 1 h. Subsequently, the glass was tempered and allowed to dry for at least 3 h at 150 °C. To improve homogenization, the glass frit was melted under the above conditions, tempered, and dried a second time. The homogeneous glass grains were milled in a dry state and sieved (<85 μm). Powdered glass with grains measuring an average 20 μm was produced in this way.

Next, monolithic glass-ceramic ingots were produced in a reactive sintering process. First, cylinders measuring 13 mm in diameter and 12–20 mm in height were formed by pressing the powdered glass in a uniaxial press at 750 bar. The subsequent sintering process had do be adjusted to the composition of the two types of glass. For example, the dimensional stability of the cylinder had to be assured. Additionally, the sintering process had a considerable influence on the crystallization of the glasses. The sintering temperatures were 790 (glass-ceramic A) and 950 °C (glass-ceramic B). These temperatures were held for 40 (A) and 10 (B) min under vacuum (see Fig. 1).

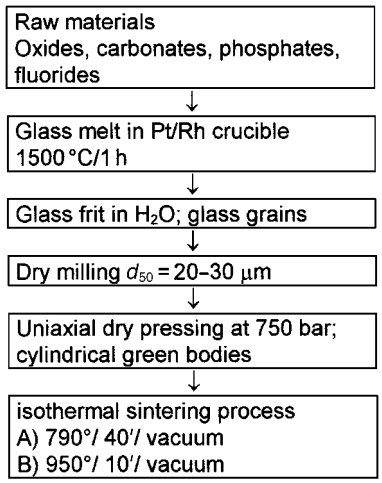

Figure 1 Flow diagram showing the processing of sintered glass-ceramic ingots.

2.3. Preparation of test specimens

The two glass-ceramics A and B were characterized by measuring the 3-point bending strength, the fracture toughness, the modulus of elasticity, the Vickers hardness, the bonding strength to TZP-ceramic, the coefficient of thermal expansion and the translucency.

The sintered glass-ceramic ingots were moulded into the desired shape using the lost wax technique in a process combining heat and pressure. A wax model was produced in 1 : 1 scale and embedded in a special investment material (IPS Empress® Special Investment Material for Staining Technique, Ivoclar Ltd, Schaan, Liechtenstein). The mould was then hardened at 850 °C without shrinkage. The wax model was burned out without leaving any traces. The hot-press furnace used (EP500, Ivoclar Ltd, Schaan, Liechtenstein) is shown in Fig. 2.

The cold glass-ceramic ingots were directly heated to the pressing temperature in the preheated mould. They were held in a vacuum at this temperature for a suitable period of time. Subsequently, the automatic moulding cycle with a pressing power of 200–300 N began. The high temperature and the pressure buildup forced the glass-ceramic into the mould.

During the hot-pressing procedure (see Table II) and the cooling phase, the final microstructure of the

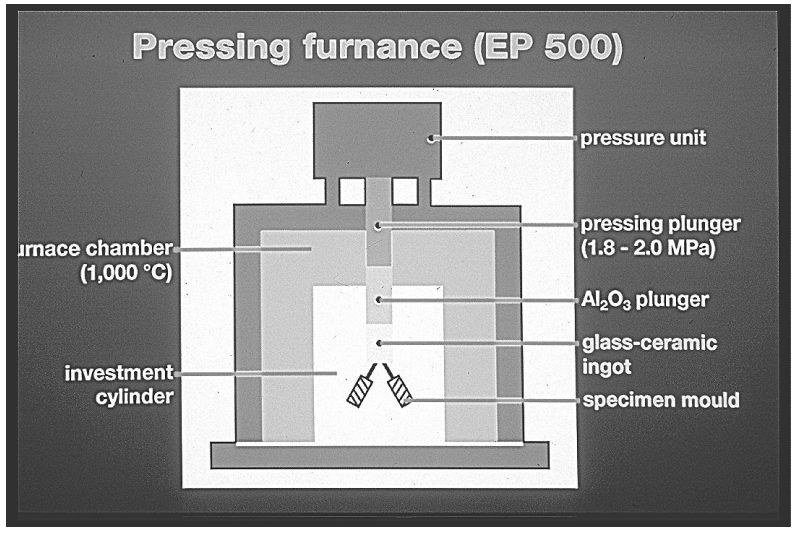

Figure 2 Schematic diagram of the EP500 hot-press furnace used to produce dental restorations and physical test samples.

TABLE II Hot-pressing parameters for glass-ceramic A and B

	Pressing temperature (°C)	Pressing power (MPa)	Holding time at pressing temperature (min)	Vacuum (mbar)
Glass-ceramic A	900	2	15–20	50
Glass-ceramic B	1000	2	20–25	50

glass-ceramic was formed. Once the moulding cycle had ended, the mould was left to cool to room temperature. Subsequently, the pressed part was divested from the mould by blasting the mould material with corundum powder and glass beads at 1–2 bar pressure.

The above procedure was used to prepare specimens in the required dimensions for the following tests:

- Three-point bending strength: $1.2 \times 4.0 \times 20$ mm^3 (according to ISO 6872-1995 "Dental ceramic")
- Fracture toughness K_{Ic}: $1.4 \times 4.0 \times 20$ mm^3 according to the SENB (single edge notched beam) method Test instructions and calculations according to DIN 51109 and ASTM E399 Three-point bending strength test with a span of 15 mm; notch <150 μm; depth of cut of 2 mm
- Modulus of elasticity: Evaluated by means of the stress-strain diagram of the three-point flexural test
- Vickers hardness: according to (ISO 6507)
- Strength of the bond between the glass-ceramic and the ZrO_2 ceramic
- Coefficient of linear thermal expansion
- Contrast value measurements as a standard for the translucency of the material (BS 5612: 1978 test standard for dental ceramics); thickness of sample, 1.1 mm; diameter of sample, 16 mm; surface, 1 μm polished.
- Microstructural analysis on fractured and etched surfaces.

The three-point flexural strength, modulus of elasticity, and fracture toughness were determined with the Zwick 1445 universal testing equipment. The hardness was established with a Vickers pyramid on a polished sample surface using 9.81 N test force. The bonding strength was determined in a push-out test on a glass-ceramic ring pressed to a post. A Netzsch dilatometer (DIL 402C) was used to measure the coefficient of linear thermal expansion. The contrast value was established using the contrast method and a Minolta CR 300. Microstructural analyses were conducted on an etched fracture surface using SEM (Zeiss DSM 962) and phase analysis was carried out with X-ray diffraction (XRD).

Monolithic glass samples were studied to determine the crystal growth rates as a function of time and temperature. Since these samples were not produced by sintering and hot-pressing, they were considered to be of model specimens.

3. Results

3.1. Microstructural examinations

3.1.1. Glass-ceramic A containing 15 wt% ZrO_2 and 4 wt% P_2O_5

3.1.1.1. Microstructure of the ingots. When the glass-powder was sintered at 790 °C for 40 min, a glass-ceramic was produced by controlled crystallization. The main crystalline phase was composed of very small β-Li_3PO_4 crystals [16]. These crystals were formed in a droplet phase, which was rich in phosphate, by liquid-liquid phase separation in the volume of the glass. As a result of isothermal heat treatment, these droplets grew or clustered together, ultimately forming the very small β-Li_3PO_4 crystals. Fig. 3 shows the microstructure after

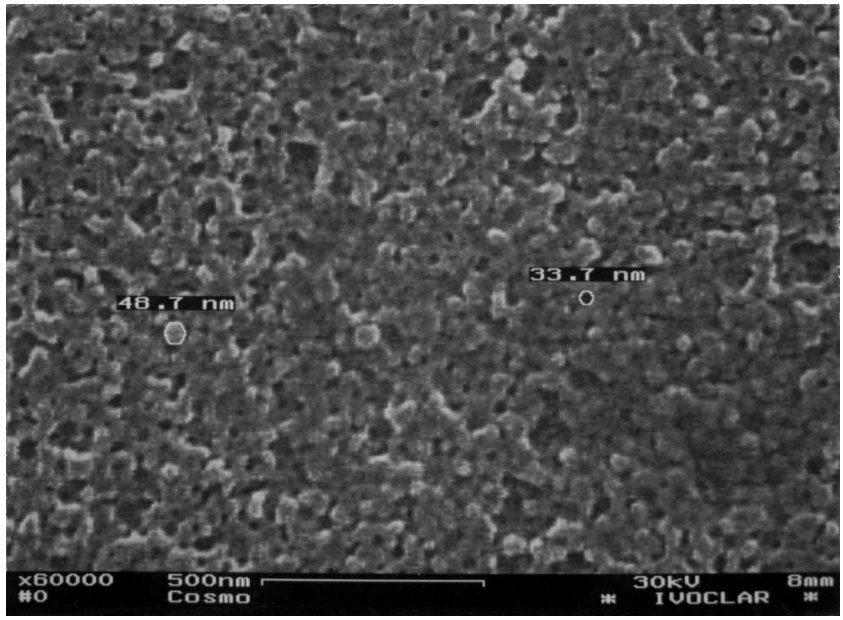

Figure 3 Microstructure of a sintered ingot made of glass-ceramic A showing β-Li_3PO_4 crystals measuring less than 50 nm in diameter (fracture surface etched with 3% HF for 10 s).

the material has been etched. The Li_3PO_4 crystals were dissolved from the surface by etching with 3% HF-solution. The size of the crystallites was established on the basis of the pitted surface structure. They measured less than 50 nm in diameter.

Additional crystalline phases such as ZrO_2 and $ZrSiO_4$ were not detected in XRD analyses. These phases may have been amorphous on the X-ray because of their very small size.

The very small β-Li_3PO_4 crystals were responsible for the high translucency of the ingots. Opaqueness caused by light diffraction and refraction was only found in a very small number of instances.

3.1.1.2. Microstructure of the pressed ceramic. By hot-pressing the ingots at 900 °C, growth of the droplet shaped β-Li_3PO_4 crystals was observed. The crystals had a diameter of 0.2–0.5 μm. In Fig. 4, the β-Li_3PO_4 crystals are represented by the dark holes in the glass matrix. The crystals were dissolved by etching with HF. The $Li_2ZrSi_6O_{15}$ ($Li_2O{\cdot}ZrO_2{\cdot}6\ SiO_2$) or $LiNaZrSi_6O_{15}$ crystals occurred as a crystal phase containing ZrO_2 [17]. The XRD pattern of $Li_2ZrSi_6O_{15}$ was similar to the patten of $LiNaZrSi_6O_{15}$. The monoclinic pseudo-orthorhombic rod-like crystals were clustered in spherical agglomerates. The diameter of the agglomerates measured between 5 and 10 μm (Fig. 5).

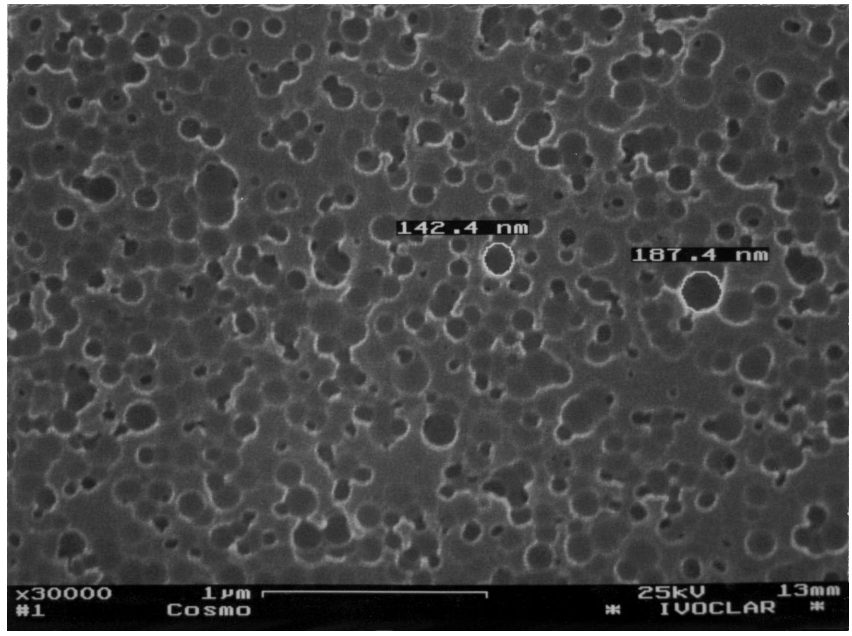

Figure 4 Microstructure of an ingot A hot-pressed at 900 °C containing β-Li_3PO_4 droplet phases measuring 100–200 nm (fracture surface, 3% HF, 10 s).

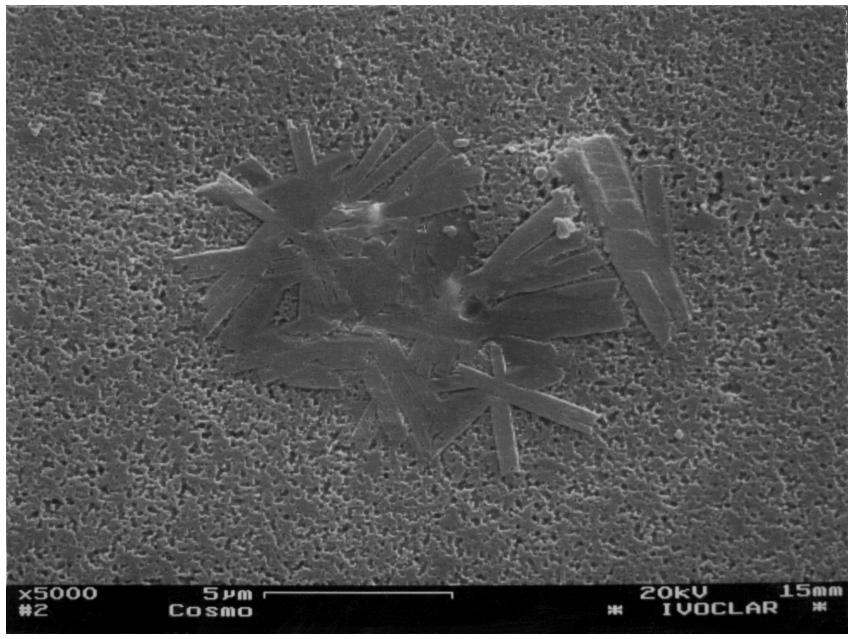

Figure 5 Microstructure of an ingot A hot-pressed at 900 °C containing also agglomerated $Li_2ZrSi_6O_{15}$ or $LiNaZrSi_6O_{15}$ crystals (fracture surface, 3% HF, 10 s).

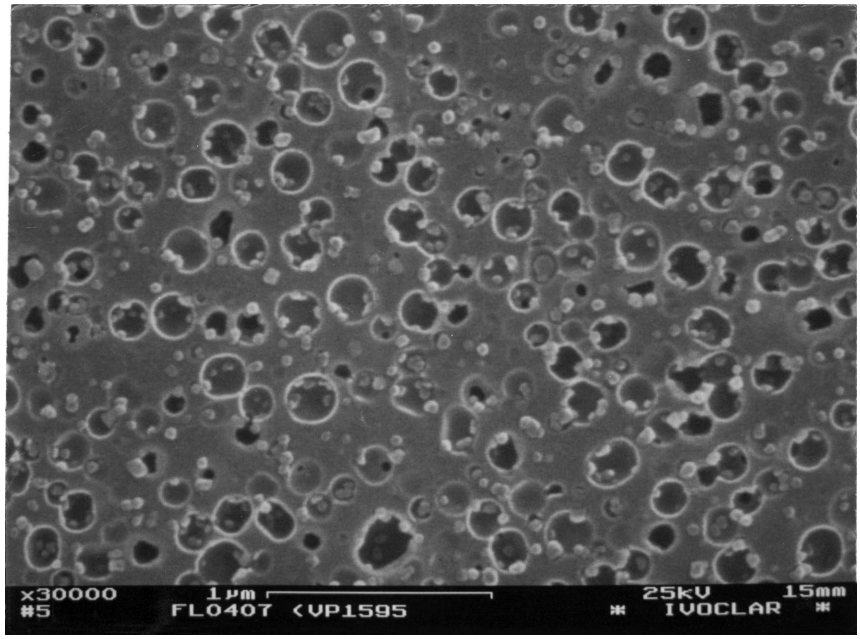

Figure 6 Microstructure of a sintered ingot made of glass-ceramic B with Li_3PO_4 droplet phase measuring 300–400 nm in diameter (fracture surface, 3% HF, 10 s).

3.1.2. Glass-ceramic B containing 20 wt % ZrO_2 and 10 wt % P_2O_5

3.1.2.1. Microstructure of the ingots. The glass-ceramic was produced in a reactive sintering process at 950 °C by controlled crystallization. Li_3PO_4 and ZrO_2 (monoclinic and orthorhombic/tetragonal) were detected by XRD analysis. Both crystal phases were formed by volume crystallization. The Li_3PO_4 crystals developed from amorphous droplets measuring approximately 100 nm in diameter. These droplets, which were rich in P_2O_5 , had been formed by liquid-liquid phase separation. The droplet phase began to grow with increasing heat treatment. The droplets grew and clustered to form droplets with a diameter of 300–400 nm, demonstrating a crystalline structure (Fig. 6). Given this heterogeneous structure and the size of the droplets in the wave range of visible light, the ingot demonstrated a milky white colour and low translucency.

3.1.2.2. Microstructure of the hot-pressed glass-ceramic. By hot-pressing the ingot at 1000 °C for 25 min, a new microstructure and, hence, a new material with different properties was formed, containing different crystal phases.

- Formation of β-Li_3PO_4 crystals: During the hot-press procedure, the droplet shaped phase continued to grow and form β-Li_3PO_4 crystals according to their orthorhombic crystal system. The size of the crystals growing along the *c* axis measured less than 5 μm; along the *a* and *b* axes less than 2 μm. The crystals were formed by volume crystallization. In Fig. 7, the Li_3PO_4 crystals have been dissolved from the surface of the glass matrix with HF etching. The black holes provide an indication of the habit and size of the Li_3PO_4 crystals.
- Formation of ZrO_2 crystals: ZrO_2 crystals were precipitated near the phase boundary of Li_3PO_4 crystals as well as in the glass matrix. Crystals were formed by volume crystallization. Monoclinic as well as orthorhombic/tetragonal modifications were identified in the XRD spectra. The tetragonal ZrO_2 crystals measured less than 150 nm. As a result, it was difficult to classify the modifications as either monoclinic or tetragonal in the XRD spectra. On the basis of the bright contrast, needle-like monoclinic ZrO_2 crystals as well as the very small ZrO_2 crystals were identified in the composition contrast image (Fig. 8).
- Formation of zirkon mineral $ZrSiO_4$($ZrO_2 \cdot SiO_2$): $ZrSiO_4$ formed as a new crystal phase in the hot-pressing procedure. The crystals were tetragonal [18]. Comparative tempering of sintered and monolithic glass samples demonstrated that $ZrSiO_4$ was formed by surface crystallization. When monolithic glass samples were tempered at 950 and 1050 °C, $ZrSiO_4$ was not found.

Kinetic investigations of the crystal growth of ZrO_2 and Li_3PO_4 in monolithic samples of glass-ceramic B demonstrated that there was no time lag between nucleation and crystal growth. Moreover, all the crystal phases demonstrated very high growth rates up to a temperature of 1050 °C [6]. Crystal growth rates as a function of temperature are listed in Table III. The growth of $ZrSiO_4$ crystals could not be studied in monolithic glass

TABLE III Crystal growth rates of glass-ceramic B as a function of temperature

Temperature °C	950	1050
Orthorhombic Li_3PO_4 crystals [$\mu m \cdot h^{-1}$]	0.25	4.0
ZrO_2 microcrystals [$\mu m \cdot h^{-1}$]	0.1	0.2
Monoclinic needle-like ZrO_2 crystals [$\mu m \cdot h^{-1}$]	3.5	5.0

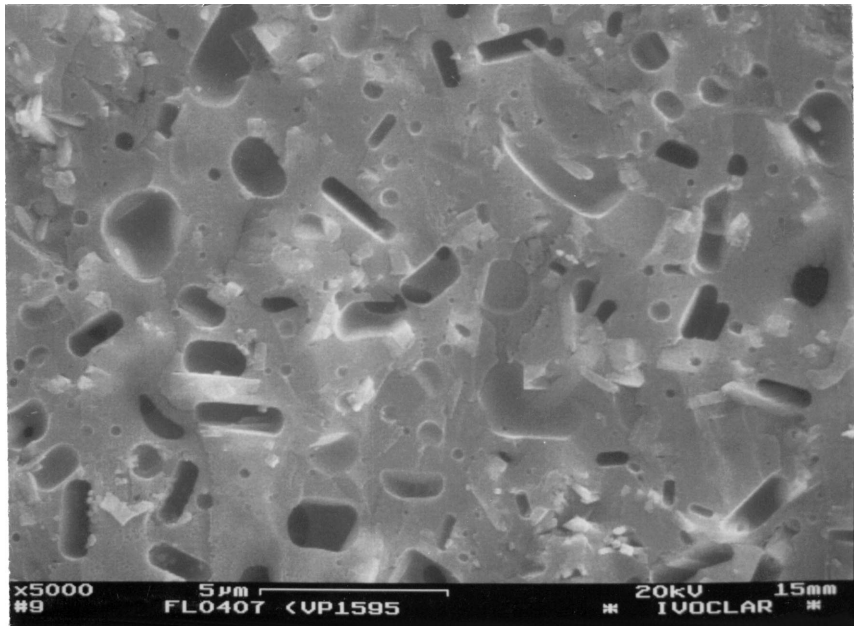

Figure 7 Microstructure of glass-ceramic B hot-pressed at 1000 °C; dark holes correspond to the dissolved Li_3PO_4 crystals (fracture surface, 3% HF, 10 s).

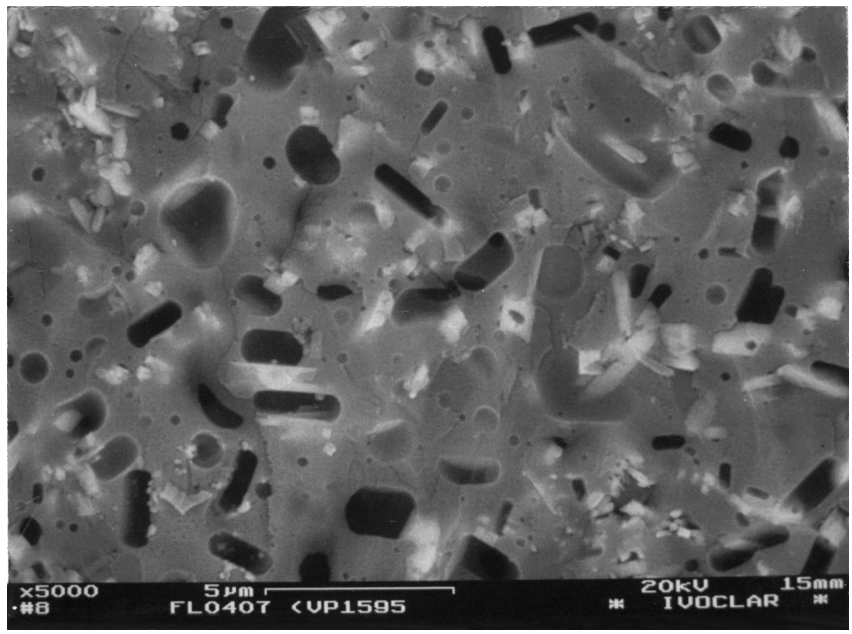

Figure 8 Composition contrast image of ZrO_2 crystals (white image).

samples, since crystallization occurred in the form of surface crystallization.

3.2. Properties of the glass-ceramics

The properties of glass-ceramic A and B were achieved by controlled crystallization during the sintering and hot-pressing procedures. The different compositions were responsible for producing the particular microstructures. The material properties such as strength and translucency were specifically adjusted in the microstructure of the glass-ceramics. Table IV shows the properties of the two glass-ceramics and of TZP-ceramic.

In glass-ceramic B, crack deflection at Li_3PO_4 crystals was observed. In Fig. 9, crack progression starting from a Vickers hardness indentation is visible. The crack was deflected by β-Li_3PO_4 crystals (dark contrast). The deflection mechanism hindered the growth of the crack, since additional energy for the development of the fracture surface was expended.

3.3. Properties of the bond between glass-ceramic A and TZP ceramic

In Figs 10 and 11, the homogeneous bond between glass-ceramic A and the TZP post is distinct. Neither on a macroscopic level in a polished cross section, nor on a microscopic level in a fracture surface were cracks or porous areas detected, which may have been caused by thermal stress in the cooling phase or by a chemical reaction.

TABLE IV Properties of glass-ceramic A and B and of TZP ceramic

	Glass-ceramic A	Glass-ceramic B	TZP ZrO_2 ceramic stabilized with 3 mol % Y_2O_3 [8]
Mechanical properties			
Three-point flexural strength (MPa)	164 ± 26	260 ± 39	900
K_{Ic} (SENB) (MPa$\sqrt{}$m)	1.1 ± 0.1	1.9 ± 0.1	7
Modulus of elasticity (GPa)	55	59	210
Vickers hardness (MPa)	5340	6350	12000
Strength of the bond with TZP [19]	35 ± 9	39 ± 16	—
Optical properties			
Contrast ratio CR	Without		
(0 ≅ 100% transparent	pigments: 0.19;	0.99	0.71
1 ≅ 100% opaque)	with pigments: 0.72		
Thermal properties			
Coefficient of linear thermal expansion (100–500 °C) (in K^{-1})	9.4×10^{-6}	9.7×10^{-6}	10.7×10^{-6}
Glass transition temperature (°C)	544	617	—

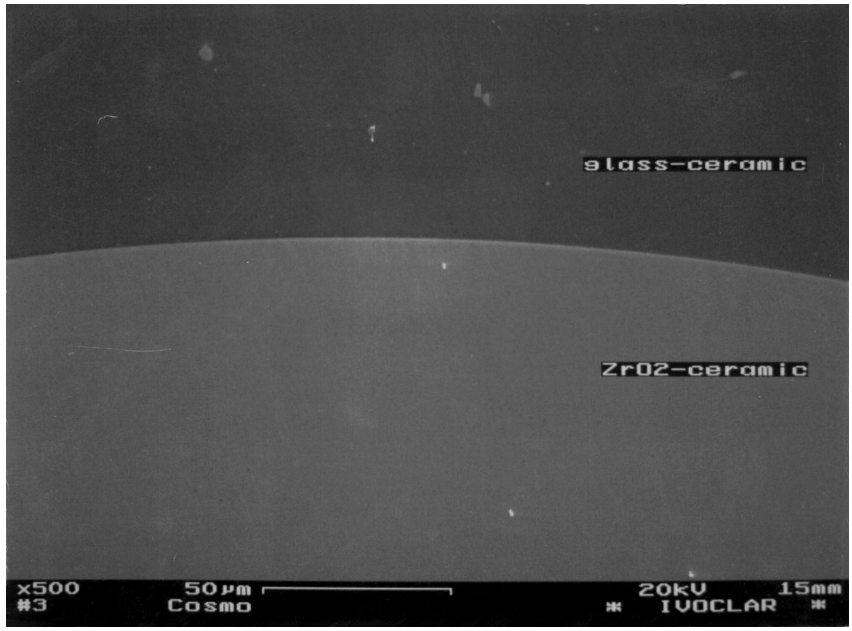

Figure 9 Macroscopic (×500) image of the defect-free bond between glass-ceramic A and the TZP-ceramic after hot-pressing at 900 °C (SEM images, polished).

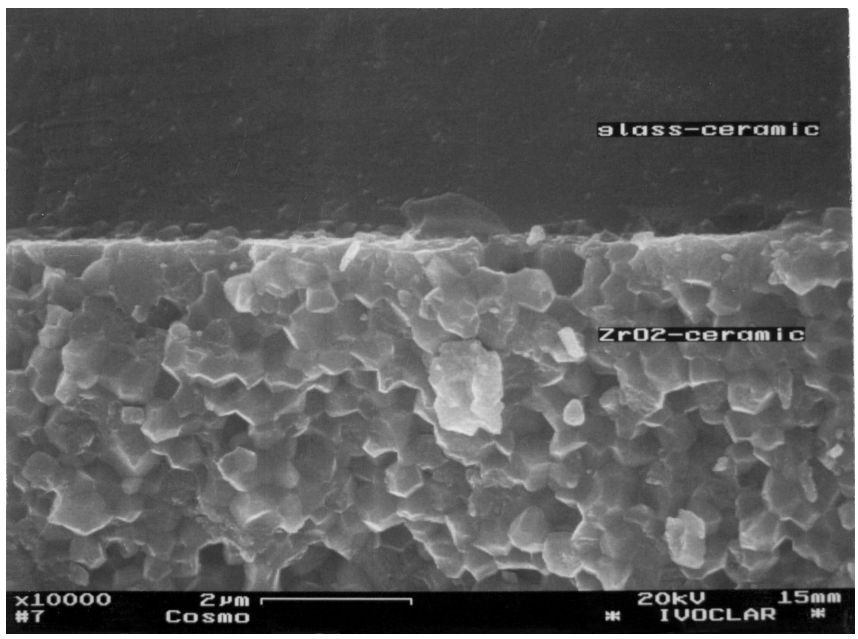

Figure 10 Microscopic (×10 000) image of the defect-free bond between glass-ceramic A and the TZP-ceramic after hot-pressing at 900 °C (SEM images, fracture surface).

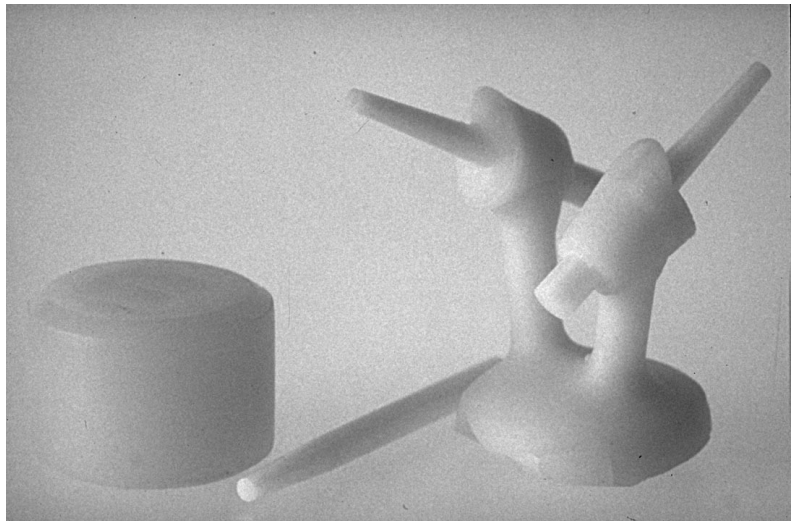

Figure 11 Ingot, cylindrical ZrO_2 post with a conical tip, and an all-ceramic core buildup produced in a hot-pressing procedure using glass-ceramic A.

3.4. Dental applications

Both glass-ceramic A and B were successfully bonded to a prefabricated cylindrical TZP post with a conical tip in a hot-pressing procedure. The surface roughness of the TZP posts, the high content of ZrO_2 in the glass-ceramic, and the adjusted coefficient of thermal expansion produced bonding strengths of 35 and 39 MPa [19]. In dental adhesive technology, these values are considered to be highly satisfactory. Typical bonding strength values of natural teeth and dental composite materials were in the range of 20–25 MPa [20]. Because of its favourable physical properties, this composite system was found to be suitable for producing dental root posts. The glass-ceramic was used to replace the missing dentin, while the TZP post with the conical tip adhesively cemented in the root canal was used to anchor and secure the restoration. The excellent translucency of glass-ceramic A allowed the all-ceramic core buildups to be used in the anterior region, where aesthetics play a decisive role (Figs 12 and 13). To finish the restoration, a ceramic crown was seated on the glass-ceramic dentin material using the adhesive technique. Consequently, a biocompatible ceramic or glass-ceramic dental restoration was achieved.

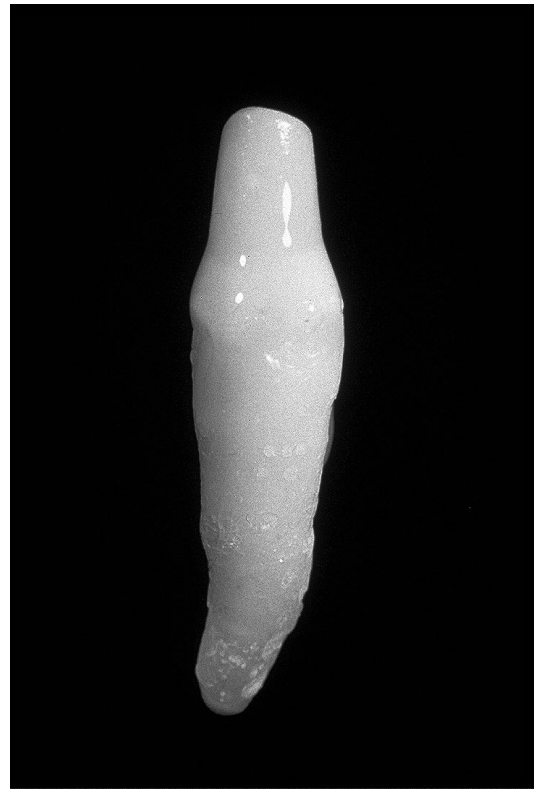

Figure 12 All-ceramic core buildup on a treated root canal (made by H.P. Foser, Ivoclar Ltd, Schaan, Liechtenstein).

4. Discussion

Glass-ceramic A and B had different microstructures. The temperatures during the sintering and hot-pressing procedure were mainly determined by the different amounts of ZrO_2 and P_2O_5. Glass-ceramic A with smaller amounts of ZrO_2 and P_2O_5 was pressed at a lower temperature of 900 °C than glass-ceramic B with higher amounts of ZrO_2 and P_2O_5. The higher pressing temperature of 1000 °C and the larger amounts of ZrO_2 and P_2O_5 in glass-ceramic B produced a correspondingly higher crystalline content and, beside Li_3PO_4, new crystalline phases like ZrO_2 (monoclinic and tetragonal) and $ZrSiO_4$. Because of the high refractive index of the ZrO_2-containing crystals in comparison to the glass matrix, glass-ceramic B was white and opaque.

Given the high crystalline content, glass-ceramic B demonstrated distinctly better strength and toughness values than glass-ceramic A. Its 3-point bending strength of 260 MPa was 63% higher than the strength of glass-ceramic A. In fact, the fracture toughness K_{Ic} of 1.9 MPa$\sqrt{m}$ was found to be 82% higher than that of glass-ceramic A.

The following mechanisms may have contributed to the reinforcement:

(a) Crack deflection by dispersion strengthening: In glass-ceramic B, crack deflection at Li_3PO_4 crystals was observed. The deflection mechanism hindered the

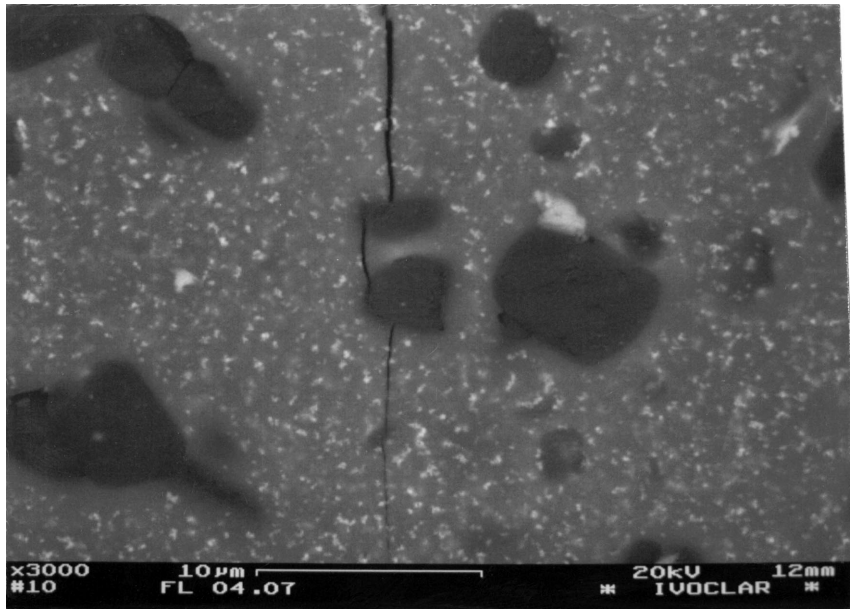

Figure 13 Crack deflection on Li_3PO_4 crystals in glass-ceramic B (polished surface, BSE compo).

growth of the crack, since additional energy for the development of the fracture surface was expanded. Dispersion strengthening was based on different moduli of elasticity and coefficients of thermal expansion between the glassy matrix and the Li_3PO_4 crystals [21].

(b) ZrO_2 crystals: Transformation reinforcement of the existing tetragonal ZrO_2 presented another strengthening mechanism. The existing non-needle-like ZrO_2 crystals, however, were at the lower limit for the tetragonal phase to be transformable. Monoclinic ZrO_2 crystals, those in needle-like form in particular, contributed to the increase in strength and toughness by dispersion strengthening. There was no microcrack toughening observed [22].

(c) Incorporation of $[Zr^{4+}]$ into the glass structure: The high content of Zr ions in the glass network structure, which produced bracing by complex $[ZrO_4]$ structural units, may represent another reinforcement mechanism.

The coefficient of linear thermal expansion was for both glass-ceramics lower than that of the ZrO_2 ceramic in the temperature range of 100–500 °C. As a result of this adjustment, a crack-free bond between the glass-ceramic and the ZrO_2 ceramic was achieved.

Because of its excellent translucency (contrast ratio of 0.72), glass-ceramic A can be used to produce all-ceramic core buildups in combination with TZP posts in anterior regions, where aesthetics plays a decisive role. The contrast ratio of glass-ceramic A (0.72) and TZP-ceramic (0.71) were nearly identical which resulted in aesthetic restorations like natural teeth. The improved mechanical properties of glass-ceramic B make the material suitable for use in the posterior region, since aesthetics and the opacity of the glass-ceramic play a lesser role in this area. Given the high stress-bearing capabilities of posterior teeth, the glass-ceramic should exhibit correspondingly high strength and toughness.

5. Conclusions

Two glass-ceramics of the SiO_2–Li_2O–ZrO_2–P_2O_5 system showed different mechanical and optical properties because of their specific content of ZrO_2 and P_2O_5. The high content of ZrO_2 (20 wt %) and P_2O_5 (10 wt %) in glass-ceramic B lead to excellent mechanical properties. The 3-point flexural strength measured 260 ± 39 MPa and the fracture toughness K_{Ic} was 1.9 ± 0.1 MPa$\sqrt{m}$. The high content of crystalline phases, such as tetragonal and monoclinic ZrO_2, $ZrSiO_4$ and Li_3PO_4, had also an influence on the optical properties of glass-ceramic B. The samples were white and opaque after preparation through heat pressing and viscous flow at 1000 °C. A reduction of the content of ZrO_2(15 wt %) and P_2O_5 (4.2 wt %) in glass-ceramic A had a remarkable influence on the optical properties. The samples were translucent after preparation through heat pressing and viscous flow at 900 °C. The content of crystalls was reduced in comparison to glass-ceramic B.The crystalline phases detected by XRD were Li_3PO_4 and $Li_2ZrSi_6O_{15}$ respectively $LiNaZrSi_6O_{15}$. Because of the lower crystallinity, glass-ceramic A had lower mechanical properties in comparison to glass-ceramic B. The 3-point flexural strength measured 164 ± 26 MPa and the fracture toughness K_{Ic} was 1.1 ± 0.1 MPa$\sqrt{m}$. Both glass-ceramics had similar coefficients of thermal expansion in the region of $9.4–9.7 \times 10^{-6}\,K^{-1}$. Therefore, it was possible to bond the glass-ceramic to ZrO_2-ceramic (3Y-TZP) through a hot-pressing procedure. Bonding strength of 35–39 MPa could be produced. Because of its favourable physical properties, this composite system was found to be suitable for producing dental root posts. The glass-ceramic A with its high translucency similar to natural dentine was used to replace the missing dentine, while the TZP post with the conical tip adhesively cemented in the root canal was used to anchor and secure the restoration. A ceramic crown was seated on the glass-ceramic dentin material

using adhesive technique to finish the dental restoration in the anterior region.

References

1. K. H. MEYENBERG, H. LÜTHY and P. SCHÄRER, *J. Esth. Dent.* **7**(2) (1995) 73–80.
2. I. FLEMMING, P. OEDMAN and K. BRONDUM, *Int. J. Prosthodont.* **9** (1995) 131–136.
3. H. LÜTHY, P. SCHÄRER and L. GAUCKLER, Abstract IV-2, Monte Verita Conference on Biocompatible Material Systems, Ascona, Switzerland, October 1993.
4. M. SCHWEIGER, M. FRANK, V. RHEINBERGER and W. HÖLAND in, Proceedings International Symposium on Glass Problems (Istanbul, Turkey, ICG, 1996) Vol. 2, pp. 229–235.
5. M. SCHWEIGER, M. FRANK, W. HÖLAND, S. CRAMER VON CLAUSBRUCH, W. HÖLAND and V. RHEINBERGER, *Quintessence of Dental Technology* (1998), to be printed.
6. W. HÖLAND, M. FRANK, M. SCHWEIGER, S. WEGNER and V. RHEINBERGER, Glass *Science and Technology* **69** (1996) 25–33.
7. M. SIMON, *J. Phillip* **14** (1997) 95–100.
8. W. RIEGER, *Industrie Diamanten Rundschau* **2** (1993) 2–6.
9. A. G. EVANS and A. H. HEUER, *J. Amer. Ceram. Soc.* **63** (5–6) (1980) 241–248.
10. G. PARTRIDGE, C. A. ELYARD and M. J. BUDD, in "Glasses and Glass-Ceramics." edited by M. H. Lewis (Chapman and Hall, London, 1989) pp. 226–271.
11. L. M. ECHEVERRIA and G. H. BEALL, *Ceram. Trans.* **22** (1991) 235–244.
12. M. I. BUDD, *J. Mater. Sci.* **28** (1993) 1007–1014.
13. T. UNO, T. KASUGA, S. NAKAYAMA *et al.*, *J. Amer Ceram. Soc.* **76**(2) (1993) 539–541.
14. W. SEMAR and W. PANNHORST, *Silic. Ind.* **56**(3/4) (1991) 71–75.
15. W. RIEGER and M. SCHWEIGER, *Industrie Diamanten Rundschau* **31**(4) (1997) 326–330.
16. C. KEEFER, A. MIGHELL, F. MAUER, H. SWANSON and S. BLOCK, *Inorg. Chem.* **6** (1967) 119–125.
17. P. QUINTANA and A. R. WEST, *Mineralogical Magazine* **44** (1981) 361–362.
18. W. A. DEER, R. A. HOWIE and J. ZUSSMAN (eds.), "Rock-Forming Minerals, Vol. 1A; Orthosilicates" (1982) pp. 418–442.
19. Y. KAKEHASHI, H. LÜTHY, A. WOHLWEND, LÖFFEL and P. SCHÄRER, Poster presentation, 1997 IADR/CED 34th Annual Meeting, Madrid.
20. U. SALZ, *Ivoclar-Vivadent Report* **10** (1994) 9–20.
21. K. T. FABER and A. G. EVANS, *Acta Metall.* **4** (1983) 565–576.
22. R. D. SARNO and M. TOMOZAWA, *J. Mater. Sci.* **30** (1995) 4380–4388.

Received 28 January
and accepted 22 June 1998